

# Gliding vertex on the horizontal bounding box for multi-oriented object detection

Yongchao Xu, Mingtao Fu, Qimeng Wang, Yukang Wang, Kai Chen,  
Gui-Song Xia *Senior Member, IEEE*, Xiang Bai *Senior Member, IEEE*

**Abstract**—Object detection has recently experienced substantial progress. Yet, the widely adopted horizontal bounding box representation is not appropriate for ubiquitous oriented objects such as objects in aerial images and scene texts. In this paper, we propose a simple yet effective framework to detect multi-oriented objects. Instead of directly regressing the four vertices, we glide the vertex of the horizontal bounding box on each corresponding side to accurately describe a multi-oriented object. Specifically, We regress four length ratios characterizing the relative gliding offset on each corresponding side. This may facilitate the offset learning and avoid the confusion issue of sequential label points for oriented objects. To further remedy the confusion issue for nearly horizontal objects, we also introduce an obliquity factor based on area ratio between the object and its horizontal bounding box, guiding the selection of horizontal or oriented detection for each object. We add these five extra target variables to the regression head of fast R-CNN, which requires ignorable extra computation time. Extensive experimental results demonstrate that without bells and whistles, the proposed method achieves superior performances on multiple multi-oriented object detection benchmarks including object detection in aerial images, scene text detection, pedestrian detection in fisheye images.

**Index Terms**—Object detection, R-CNN, multi-oriented object, aerial image, scene text, pedestrian detection.

## 1 INTRODUCTION

OBJECT detection has achieved a considerable progress thanks to convolutional neural networks (CNNs). The state-of-the-art methods [1], [2], [3] usually aim to detect objects via regressing horizontal bounding boxes. Yet multi-oriented objects are ubiquitous in many scenarios. Examples are objects in aerial images and scene texts. Horizontal bounding box does not provide accurate orientation and scale information, which poses problem in real applications such as object change detection in aerial images and recognition of sequential characters for multi-oriented scene texts.

Recent advances in multi-oriented object detection are mainly driven by adaption of classical object detection methods using rotated bounding boxes [4], [5] or quadrangles [6], [7], [8] to represent multi-oriented objects. Though these existing adaptions of horizontal object detection methods to multi-oriented object detection have achieved promising results, they still face some limitations. For detection using rotated bounding boxes, the accuracy of angle prediction is critical. A minor angle deviation leads to important IoU drop, resulting in inaccurate object detection. This problem is more prominent for detecting long oriented objects such as bridges and harbors in aerial images and Chinese text lines in scene images. The methods based on quadrangle regression usually have ambiguity in defining the ground-truth order of four vertices, yielding unexpected

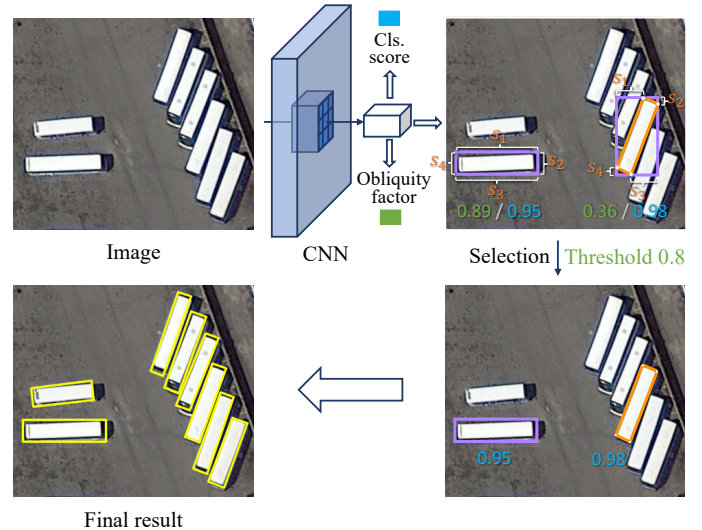


Fig. 1. Pipeline of the proposed method. An image is fed into a CNN, which outputs a classification score (blue value), a horizontal bounding box, four length ratios between each segment  $s_i$  and corresponding side, and an obliquity factor (green value) for each detection. Based on obliquity factor, we select horizontal box (in purple) or oriented detection (in orange) as the final result. Best viewed in electronic version.

detection results for objects of some orientations.

Some other methods [9], [10], [11] alternatively detect horizontal object parts followed by a grouping process. Yet, such grouping process step is usually heuristic and time-consuming. Describing an oriented object as its segmentation mask [12] is another alternative solution. However, this often results in split and/or merged components, requiring a heavy and time-consuming post-processing.

In this paper, we propose a simple yet effective frame-

- Y. Xu, M. Fu, Q. Wang, Y. Wang, and X. Bai are with the School of Electronic Information and Communications, Huazhong University of Science and Technology (HUST), Wuhan, 430074, China.  
E-mail: {yongchaoxu, mingtaofu, qimengwang, wangyk, xbai}@hust.edu.cn.
- G. S. Xia is with LIEMARS, Wuhan University.  
E-mail: guisong.xia@whu.edu.cn.
- K. Chen is with Shanghai Jiaotong University; Onyou Inc.  
E-mail: kchen@sjtu.edu.cn.

work to deal with multi-oriented object detection. Specifically, we propose to glide each vertex of the horizontal bounding box on the corresponding side to accurately describe a multi-oriented object. This results in a novel representation by adding four gliding offset variables to classical horizontal bounding box representation. Put it simply, we regress four length ratios that characterize the relative gliding offset (see Fig. 1) on each side of horizontal bounding box. Such representation may be less sensitive to offset prediction error than angle prediction error in rotated bounding box representation. By limiting the offset on the corresponding side of horizontal bounding box, we may facilitate offset learning and also avoid the confusion for sequential label points in directly regressing the four vertices of oriented objects. To further get rid of confusion issue for nearly horizontal objects, we also introduce an obliquity factor based on area ratio between the multi-oriented object and its horizontal bounding box. As depicted in Fig. 1, this obliquity factor guides us to select the horizontal detection for nearly horizontal objects and oriented detection for oriented objects. It is noteworthy that the proposed method only introduces five additional target variables, requiring ignorable extra computation time.

In summary, the main contribution of this paper are three folds: 1) We introduce a simple yet effective representation for oriented objects, which is rather robust to offset prediction error and does not have the confusion issue. 2) We propose an obliquity factor that effectively guides the selection of horizontal detection for nearly horizontal objects and oriented detection for others, remedying the confusion issue for nearly horizontal objects. 3) Without bells and whistles (*e.g.*, cascade refinement or attention mechanism), the proposed method outperforms some state-of-the-art methods on multiple multi-oriented object detection benchmarks.

The rest of this paper is organized as follows. We shortly review some related works in Section 2. We then detail the proposed method in Section 3, followed by extensive experimental results in Section 4. Finally, we conclude and give some perspectives in Section 5.

## 2 RELATED WORK

We first review some representative general object detection methods in Section 2.1. The interested readers can refer to [13] for a more complete review. Some specific and related tasks of object detection are then shortly reviewed in Section 2.2, 2.3, and 2.4. The comparison of the proposed method with some related works is discussed in Section 2.5.

### 2.1 Deep general object detection

Object detection aims to detect general objects in images with horizontal bounding boxes. Recently, many CNN-based methods have been proposed, and can be roughly summarized into top-down and bottom-up methods.

Top-down methods directly detect entire objects. They can be further categorized into two classes: two-stage and single-stage methods. R-CNN and its variances [1], [14], [15] are representative two-stage methods. They first generate proposals with selective search [16] or RPN [1] and then use the features of these proposals to predict object

categories and refine the bounding boxes. Dai *et al.* [17] propose position-sensitive score maps to address a dilemma between translation-invariance in image classification and translation-variance in object detection. Lin *et al.* [3] focus on the scale variance of objects in images and propose Feature Pyramid Network (FPN) to handle objects at different scales. YOLO and its variances [2], [18], [19], SSD [20], and RetinaNet [21] are representative single-stage methods. They predict bounding boxes directly from deep feature maps instead of region proposals, resulting in improved efficiency.

Bottom-up methods rise recently by predicting object parts followed by a grouping process. CornerNet [22], ExtremeNet [23], and CenterNet [24] are recently proposed in succession. They attempt to predict some keypoints of objects such as corners or extreme points, which are then grouped into bounding boxes. Center points are also used by [23], [24] as supplemental information for grouping.

### 2.2 Object detection in aerial images

Object detection in aerial images is challenging because of huge scale variations and arbitrary orientations. Extensive studies have been devoted to this task. The baselines on the popular dataset DOTA [25] replace horizontal box regression of faster R-CNN with regression of four vertices of quadrangle representation. Many methods resort to rotated bounding box representation. Rotated RPN is exploited in [26], [27], which involves more anchors and thus requires more runtime. Ding *et al.* [5] propose an ROI transformer that transforms horizontal proposals to rotated ones, on which the rotated bounding box regression is performed. Azimi *et al.* [28] adopt an image-cascade network to extract multi-scale features. Yang *et al.* [29] employ multi-dimensional attention to extract robust features, better coping with complex backgrounds. Zhang *et al.* [30] propose to learn global and local contexts together to enhance the features.

### 2.3 Oriented scene text detection

Oriented scene text detection has attracted great attention. It is a challenging problem due to arbitrary orientations and long text lines in particular for non-Latin texts such as Chinese. CNN-based detectors are the mainstream methods which can be roughly divided into regression-based and segmentation-based [12], [31] methods. We shortly review related regression-based methods in the following.

Most multi-oriented scene text detectors directly predict entire texts using rotated bounding box or quadrangle representation. Ma *et al.* [32] employ rotated RPN in the framework of faster R-CNN [1] to generate rotated proposals and further perform rotated bounding box regression. Liu *et al.* [33] propose to use quadrangle sliding windows to match texts with perspective transformation. TextBoxes++ [6] adopts vertex regression on SSD [20]. RRD [34] further improves TextBoxes++ [6] by decoupling classification and bounding box regression on rotation-invariant and rotation-sensitive features, respectively, making the regression more accurate for long texts. Both EAST [4] and Deep direct regression [7] perform rotated bounding box regression and/or vertex regression at each location.

## 2.4 Pedestrian detection in fisheye images

Pedestrian detection in fisheye images is different from the general pedestrian detection because pedestrians in fisheye images are commonly multi-oriented. Seidel *et al.* [35] propose to transform omnidirectional images into perspective ones, on which the detection is applied. Such transformation introduces extra computation time. Based on the prior knowledge that objects in fisheye images are radial, Tamura *et al.* [36] propose to train a general object detector with rotated images and then determine the orientations with the centers of objects and image.

## 2.5 Comparison with related works

Compared with the related works, the proposed method targets on general and ubiquitous multi-oriented object detection with a simple yet effective framework. By gliding the vertex of horizontal bounding box on each corresponding side and a novel divide-and-conquer selection scheme for nearly horizontal and oriented objects, the proposed method may better learn the offset for accurate multi-oriented object detection and does not suffer from confusion issue. Furthermore, the proposed method may be complementary and easily plugged into many existing methods focusing on enhancing features. To equip them with the proposed approach, we only need to replace rotated bounding box or vertex regression by regressing the four length ratios and obliquity factor in addition to horizontal bounding box. Such modification requires ignorable extra runtime.

## 3 PROPOSED METHOD

### 3.1 Overview

CNN-based object detectors perform well on detecting horizontal objects but struggle on oriented ones, in particular for long and dense oriented objects. Direct adaption using rotated bounding box  $B_r$  regression tends to produce inaccurate results due to high sensitivity to angle prediction error. Regressing the four vertices of quadrangle representation does not suffer from this problem, but also fails on some cases because of the ambiguity in defining the order of four ground truth vertices to be regressed. We attempt to solve the general multi-oriented object detection by introducing a simple representation for oriented objects and a novel detection scheme that divides and conquers nearly horizontal and oriented object detection, respectively. Specifically, we propose to glide the vertex of horizontal bounding box  $B_h$  on each corresponding side to accurately describe an oriented object. Put it simply, in addition to  $B_h$ , we compute four length ratios that characterize the relative gliding offset on each side of  $B_h$ . Besides, We also introduce an obliquity factor based on area ratio between multi-oriented object and its horizontal bounding box  $B_h$ . Based on the estimated obliquity factor, we select the horizontal (*resp.* oriented) detection for a nearly horizontal (*resp.* oriented) object. This simple yet effective framework only introduces five target variables compared with classical horizontal object detectors, requiring ignorable extra computation time.

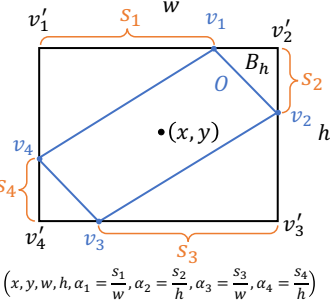


Fig. 2. Illustration of proposed representation for an oriented object  $O$  based on four intersecting points  $\{v_i\}$  between  $O$  and its horizontal bounding box  $B_h = (v'_1, v'_2, v'_3, v'_4) = (x, y, w, h)$ . We adopt  $(x, y, w, h, \alpha_1, \alpha_2, \alpha_3, \alpha_4)$  to represent oriented objects.

### 3.2 Multi-Oriented object representation

The proposed method relies on a simple representation for oriented objects and an effective selection scheme. An intuitive illustration of the proposed representation is depicted in Fig. 2. For a given oriented object  $O$  (blue box in Fig. 2) and its corresponding horizontal bounding box  $B_h$  (black box in Fig. 2), let  $v_i, i \in \{1, 2, 3, 4\}$  denote top, right, bottom, left intersecting point with its horizontal bounding box  $B_h$  denoted by  $v'_i, i \in \{1, 2, 3, 4\}$ , respectively. The horizontal bounding box  $B_h$  is also usually represented by  $(x, y, w, h)$ , where  $(x, y)$  is the center, and  $w$  and  $h$  are the width and height, respectively. We propose to represent the underlying oriented object by  $(x, y, w, h, \alpha_1, \alpha_2, \alpha_3, \alpha_4)$ . The extra variables  $\alpha_i, i \in \{1, 2, 3, 4\}$  are defined as follows:

$$\begin{aligned} \alpha_{\{1,3\}} &= \|s_{\{1,3\}}\|/w, \\ \alpha_{\{2,4\}} &= \|s_{\{2,4\}}\|/h, \end{aligned} \quad (1)$$

where  $\|s_i\| = \|v_i - v'_i\|$  denotes the distance between  $v_i$  and  $v'_i$ , *i.e.*, the length of segment  $s_i = (v_i, v'_i)$  representing the gliding offset from  $v'_i$  to  $v_i$ . It is noteworthy that all  $\alpha_i$  is set to 1 for horizontal objects.

In addition to the simple representation in terms of  $(x, y, w, h, \alpha_1, \alpha_2, \alpha_3, \alpha_4)$  for an oriented object  $O$ , we also introduce an obliquity factor characterizing the tilt degree of  $O$ . This is given by the area ratio  $r$  between  $O$  and  $B_h$ :

$$r = |O| / |B_h|, \quad (2)$$

where  $|\cdot|$  denotes the cardinality. Nearly horizontal objects have a large obliquity factor  $r$  being close to 1, and the obliquity factor  $r$  for extremely slender and oriented objects are close to 0. Therefore, we can select the horizontal or oriented detection as the final result based on such obliquity factor  $r$ . Indeed, it is reasonable to represent nearly horizontal objects with horizontal bounding boxes. However, oriented detections are required to accurately describe oriented objects.

### 3.3 Network architecture

The network architecture (see Fig. 3) is almost the same as faster R-CNN [1]. We simply add five extra target variables (normalized to  $[0, 1]$  using the sigmoid function) to the head of faster R-CNN [1]. Specifically, The input image is first fed into a backbone network to extract deep features and generate bounding box proposals with RPN [1]. Then the regional features extracted via RoIAlign [37] on proposals

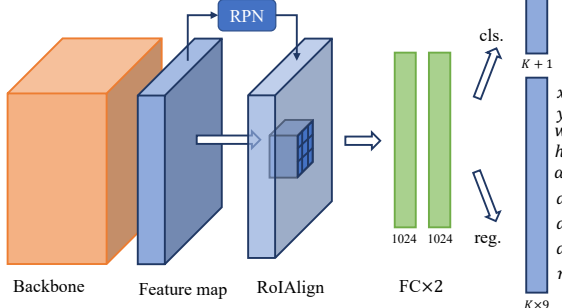


Fig. 3. Network architecture. We simply add five extra target variables (normalized to [0, 1] using the sigmoid function) to the head of faster R-CNN [1].  $K$ : number of classes;  $k$ : a certain class.

are passed through a modified R-CNN head to generate final results, including a horizontal bounding box  $(x, y, w, h)$ , four variables  $(\alpha_1, \alpha_2, \alpha_3, \alpha_4)$  characterizing the oriented bounding box, and obliquity factor  $r$  that indicates whether the object is nearly horizontal or not.

### 3.4 Ground-truth generation

The ground-truth for each object is composed of three components: classical horizontal bounding box representation  $(\tilde{x}, \tilde{y}, \tilde{w}, \tilde{h})$ , four extra variables  $(\tilde{\alpha}_1, \tilde{\alpha}_2, \tilde{\alpha}_3, \tilde{\alpha}_4)$  representing the oriented object, and the obliquity factor  $\tilde{r}$ . The horizontal bounding box ground-truth follows the pioneer work in [14], which is relative to the proposal. The ground-truth for the four extra variables  $(\tilde{\alpha}_1, \tilde{\alpha}_2, \tilde{\alpha}_3, \tilde{\alpha}_4)$  and obliquity factor  $\tilde{r}$  depend only on the underlying ground-truth object, and are directly computed by Eq. (1) and (2), respectively.

### 3.5 Training objective

The proposed method involves loss for RPN stage and R-CNN stage. The loss of RPN is the same as that in [1]. The loss  $L$  for R-CNN head contains a classification loss term  $L_{cls}$  and a regression loss term  $L_{reg}$ . The R-CNN loss  $L$  is given by

$$L = \frac{1}{N_{cls}} \sum_i L_{cls} + \frac{1}{N_{reg}} \sum_i p_i^* \times L_{reg}, \quad (3)$$

where  $N_{cls}$  and  $N_{reg}$  are the number of total proposals and positive proposals in a mini-batch fed into the head, respectively, and  $i$  denotes the index of a proposal in a mini-batch. If the  $i$ -th proposal is positive,  $p_i^*$  is 1, otherwise it is 0. The regression loss  $L_{reg}$  contains three terms for horizontal bounding box, four length ratios  $(\alpha_1, \alpha_2, \alpha_3, \alpha_4)$ , and obliquity factor  $r$  regression, respectively. Put it simply, the regression loss  $L_{reg}$  is given by

$$\begin{aligned} L_{reg} &= \lambda_1 \times L_h + \lambda_2 \times L_\alpha + \lambda_3 \times L_r, \\ L_\alpha &= \sum_{i=1}^4 \text{smooth}_{L_1}(\alpha_i - \tilde{\alpha}_i), \\ L_r &= \text{smooth}_{L_1}(r - \tilde{r}), \end{aligned} \quad (4)$$

where  $L_h$  is the loss for horizontal box regression, which is the same as that in [1], and  $\lambda_1$ ,  $\lambda_2$ , and  $\lambda_3$  are hyperparameters that balance the importance of each loss term.

### 3.6 Inference

During testing phase, for a given image, the forward pass generates a set of  $(x, y, w, h, \alpha_1, \alpha_2, \alpha_3, \alpha_4, r)$  representing horizontal bounding boxes, four length ratios, and obliquity factors. For each candidate, if its obliquity factor  $r$  is larger than a threshold  $t_r$ , indicating that the underlying object is nearly horizontal, we select the horizontal bounding box  $(x, y, w, h)$  as the final detection. Otherwise, we select the oriented one given by  $(x, y, w, h, \alpha_1, \alpha_2, \alpha_3, \alpha_4)$ . An oriented non-maximum suppression (NMS) is also performed.

## 4 EXPERIMENTS

We evaluate the proposed method on multiple benchmarks: DOTA [25] and HRSC2016 [38] for object detection in aerial images, MSRA-TD500 [39] and RCTW-17 [40] for long and oriented scene text detection, and MW-18Mar [41] for pedestrian detection in fisheye images. The ablation study is conducted on DOTA [25], which is a challenging dataset for multi-oriented object detection.

### 4.1 Datasets and evaluation protocols

**DOTA** [25] is a large-scale and challenging dataset for object detection in aerial images with quadrangle annotations. It contains 2806 4000 × 4000 images and 188, 282 instances of 15 object categories: plane, baseball diamond (BD), bridge, ground field track (GTF), small vehicle (SV), large vehicle (LV), ship, tennis court (TC), basketball court (BC), storage tank (ST), soccer-ball field (SBF), roundabout (RA), harbor, swimming pool (SP) and helicopter (HC). The official evaluation protocol of DOTA in terms of mAP is used.

**HRSC2016** [38] is dedicated for ship detection in aerial images, containing 1061 images annotated with rotated rectangles. We conduct experiments for the level-1 task which detects ship from backgrounds. The standard evaluation protocol of HRSC2016 in terms of mAP is used.

**MSRA-TD500** [39] is proposed for detecting long and oriented texts. It contains 300 training and 200 test images annotated in terms of text lines. Since the training set is rather small, following other methods, we also use HUST-TR400 [42] during training. The standard evaluation protocol of MSRA-TD500 based on F-measure is used.

**RCTW-17** [40] is also a long text detection dataset, consisting of 8034 training images and 4229 test images annotated with text lines. This dataset is very challenging due to very large text scale variances. We evaluate the proposed method via the online evaluation platform in terms of F-measure.

**MW-18Mar** [41] is a multi-target pedestrian tracking dataset, in which images are taken with fisheye cameras. For each video, we extract 1 of every 17 frames and manually annotate the pedestrians with rotated rectangles. We also randomly rotate four times the test images, generating 524 training and 1216 test images. The standard miss rates at every false positive per image (FPPI) and log average miss rates (LAMRs) [43] are adopted for benchmarking.



Fig. 4. Some detection results of the proposed method on DOTA [25]. The arbitrary-oriented objects are correctly detected.

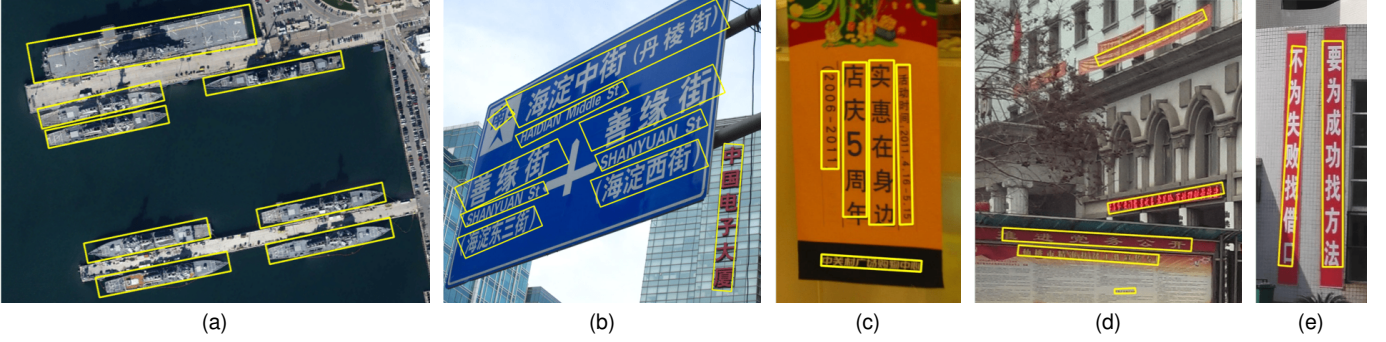


Fig. 5. Some detection results of the proposed method on HRSC2016 [38] in (a), MSRA-TD500 [39] in (b-c), and RCTW-17 [40] in (d-e).

## 4.2 Implementation Details

The proposed method is implemented based on the project of “maskrcnn\_benchmark”<sup>1</sup> using 3 Titan Xp GPUs. For a fair comparison with other methods, we adopt ResNet101 [44] for object detection in aerial images, where the batch size is set to 6 due to limited GPU memory. For the other experiments, ResNet50 is adopted, and the batch size is set to 12. In all experiments, the network is trained by SGD optimizer with momentum and weight decay set to 0.9 and  $5 \times 10^{-4}$ , respectively. The learning rate is initialized with  $7.5 \times 10^{-3}$  and divided by 10 at each learning rate decay step. The hyper-parameters  $\lambda_1$ ,  $\lambda_2$ , and  $\lambda_3$  in Eq. (4) are set to 1, 1, and 16, respectively. Without explicitly specifying, the hyper-parameter  $t_r$  on obliquity factor guiding the selection of horizontal or oriented detection is set to 0.8. Some other application related settings are depicted in the corresponding sections.

## 4.3 Object detection in aerial images

For the experiments on DOTA [25], we train the model for 50k steps, and the learning rate decays at {38k, 46k}

steps. Random rotation with angle among  $\{0, \pi/2, \pi, 3\pi/2\}$  and class balancing are adopted for data augmentation. For the experiments on HRSC2016 [38], we train the model for 3.2k steps and decay the learning rate at 2.8k steps. Horizontal flipping is applied for data augmentation. For a fair comparison, the size of training/test images and the anchor settings on both datasets are kept the same as [5].

**Overall results.** Some qualitative results on DOTA and HRSC2016 are shown in Fig. 4 and Fig. 5(a), respectively. We show all detected objects with classification scores above 0.6. As illustrated, the proposed method accurately detects both horizontal and oriented objects even under dense distribution and/or being long. The quantitative comparisons with other methods on DOTA [25] and HRSC2016 [38] are depicted in Tab. 1 and Tab. 2, respectively. Without any extra network design such as cascade refinement and attention mechanism, the proposed method outperforms some state-of-the-art methods on both DOTA and HRSC2016 and is more efficient in runtime. Specifically, For the experiment on DOTA, the proposed method without FPN [3] achieves 73.39% mAP, outperforming the state-of-the-art method [5] by 5.65% mAP. FPN [3] that exploits better multi-scale features is also beneficial for the proposed method, boosting

1. <https://github.com/facebookresearch/maskrcnn-benchmark>

TABLE 1

Quantitative comparison with other methods on DOTA. Ours- $r$  means that the divide and conquer detection scheme based on obliquity factor  $r$  is not used. \* indicates that the backbone network is light-head R-CNN [45]. † stands for evaluation using IoU threshold 0.7.

Methods	FPN	Plane	BD	Bridge	GTF	SV	LV	Ship	TC	BC	ST	SBF	RA	Harbor	SP	HC	mAP	FPS
FR-O [25]	-	79.42	77.13	17.70	64.05	35.30	38.02	37.16	89.41	69.64	59.28	50.30	52.91	47.89	47.40	46.30	54.13	-
RoI Trans.* [5]	-	88.53	77.91	37.63	74.08	66.53	62.97	66.57	79.46	76.75	59.04	56.73	62.54	61.29	55.56	67.74	5.9	
Ours*	-	<b>89.95</b>	<b>86.37</b>	45.79	73.44	<b>71.44</b>	68.20	75.96	<b>90.72</b>	<b>79.63</b>	<b>85.03</b>	58.56	<b>70.19</b>	68.28	<b>71.34</b>	54.45	72.49	8.4
Ours- $r$	-	89.93	85.78	45.90	73.66	70.07	69.10	76.78	90.62	79.08	83.94	57.75	67.57	67.53	70.85	56.46	72.33	<b>9.8</b>
Ours	-	89.89	85.99	<b>46.09</b>	<b>78.48</b>	70.32	<b>69.44</b>	<b>76.93</b>	90.71	79.36	83.80	57.79	68.35	<b>72.90</b>	71.03	<b>59.78</b>	<b>73.39</b>	<b>9.8</b>
Azimi <i>et al.</i> [28]	✓	81.36	74.30	47.70	70.32	64.89	67.82	69.98	90.76	79.06	78.20	53.64	62.90	67.02	64.17	50.23	68.16	-
RoI Trans.* [5]	✓	88.64	78.52	43.44	75.92	68.81	<b>73.68</b>	83.59	90.74	77.27	81.46	58.39	53.54	62.83	58.93	47.67	69.56	-
CADNet [30]	✓	87.80	82.40	49.40	73.50	71.10	63.50	76.60	<b>90.90</b>	79.20	73.30	48.40	60.90	62.00	67.00	<b>62.20</b>	69.90	-
R <sup>2</sup> CNN++ [29]	✓	89.66	81.22	45.50	75.10	68.27	60.17	66.83	<b>90.90</b>	80.69	86.15	<b>64.05</b>	63.48	65.34	68.01	62.05	71.16	-
RBox reg.	✓	89.37	75.96	35.43	69.57	68.35	63.78	74.92	90.76	<b>84.70</b>	85.26	62.43	62.40	52.97	60.32	54.61	68.72	9.2
Vertex reg.	✓	80.16	76.77	43.31	69.38	55.71	56.52	72.25	88.10	28.95	86.31	63.66	62.23	61.62	68.18	41.65	63.65	9.8
Ours*	✓	<b>90.02</b>	84.41	49.80	<b>77.93</b>	72.23	72.52	85.81	90.85	79.21	86.61	59.01	69.15	66.30	71.22	55.67	74.05	7.1
Ours- $r$	✓	89.40	<b>85.08</b>	52.00	77.40	72.68	72.89	86.41	90.74	78.80	86.79	57.84	70.42	67.73	<b>71.64</b>	56.63	74.43	<b>10.0</b>
Ours	✓	89.64	85.00	<b>52.26</b>	77.34	<b>73.01</b>	73.14	<b>86.82</b>	90.74	79.02	<b>86.81</b>	59.55	<b>70.91</b>	<b>72.94</b>	70.86	57.32	<b>75.02</b>	<b>10.0</b>
RBox reg.†	✓	42.52	21.76	10.47	36.53	26.57	26.91	32.39	63.20	36.56	33.54	33.04	15.63	11.16	10.05	12.98	27.56	9.2
Vertex reg.†	✓	67.94	50.51	14.28	47.46	29.79	27.92	40.66	72.75	14.29	67.59	33.47	40.87	22.04	17.91	15.13	37.51	9.8
Ours*†	✓	<b>77.98</b>	53.21	12.52	<b>68.87</b>	47.25	46.07	54.83	<b>90.45</b>	68.00	68.45	<b>56.44</b>	40.12	28.59	22.47	19.13	50.29	7.1
Ours- $r$ †	✓	67.66	50.37	<b>17.07</b>	60.60	48.74	49.00	61.59	88.98	68.84	<b>74.83</b>	48.30	48.03	32.58	23.78	23.75	50.94	<b>10.0</b>
Ours†	✓	77.32	<b>59.75</b>	15.95	67.63	<b>50.02</b>	<b>50.25</b>	<b>63.62</b>	90.38	<b>69.04</b>	74.56	51.58	<b>50.16</b>	<b>32.73</b>	<b>24.19</b>	<b>25.18</b>	<b>53.49</b>	<b>10.0</b>

TABLE 2

Quantitative comparison with some state-of-the-art methods on HRSC2016. \* indicates that Light-head R-CNN is adopted.

Methods	RC2 [46]	R <sup>2</sup> PN [27]	RRD [34]	RoI Trans.* [5]	Ours*	Ours
mAP	75.7	79.6	84.3	86.2	87.4	<b>88.2</b>

the performance to 75.02%. The proposed method using FPN [3] improves the state-of-the-art method [29] by 3.86% mAP. For HRSC2016 dataset, the proposed method achieves 88.2% mAP, improving state-of-the-art methods by 2%.

**Experiments on different network architectures.** To further demonstrate the versatility of the proposed method, we evaluate the proposed method on different networks. Concretely, we replace the faster R-CNN head by light-head R-CNN [45] head. As depicted in Tab. 1, using the same network on DOTA [25], the proposed method improves [5] by 4.49% and 4.75% mAP with and without FPN, respectively. The proposed method outperforms [5] by 1.2% mAP on HRSC2016 [38].

**Ablation study.** To further verify the effectiveness of the proposed method, we compare with two baseline methods using rotated bounding box representation (denoted by RBox reg.) and quadrangle representation (denoted by Vertex Reg.) on DOTA [25]. Some qualitative comparison can be found in Fig. 6. We rotate an image with several different angles and test the proposed method and two baseline methods on the rotated images. Rotated bounding box representation produces inaccurate results due to the imprecise angle regression. The baseline method based on regression of four vertices have difficulty for tilted objects at some orientations due to the confusion in defining the vertex order in training. The proposed method is able to accurately detect objects of any orientations.

The quantitative comparison with baseline methods is depicted in the middle of Tab. 1. The proposed method outperforms the two baseline methods by a large margin. Specifically, the proposed method outperforms the baseline using rotated bounding box regression and quadrangle regression by 6.30% and 11.37% mAP at the cost of ignorable runtime. In fact, as depicted in Tab. 1, the proposed method is more efficient than both baseline methods producing

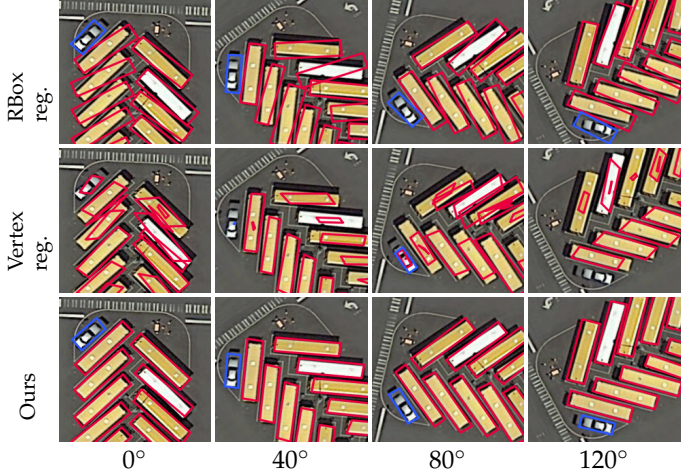


Fig. 6. Qualitative comparison with baseline methods in detecting objects of different orientations (by rotating an input image with different angles). The meaning of colors is the same as that in Fig. 4.

more false detections. To further demonstrate the accuracy of the proposed method, we also conduct a benchmark using larger IoU threshold 0.7 in the evaluation system. As shown in Tab. 1, the improvement is even more significant, changing from 6.30% (*resp.* 11.37%) to 25.93% (*resp.* 15.98%).

We also assess the individual contribution of the proposed representation for oriented objects and the divide-and-conquer detection scheme in the proposed method. To this end, we evaluate an alternative of the proposed method by discarding the divide-and-conquer detection scheme based on obliquity factor  $r$ . As depicted in Tab. 1, the proposed representation in terms of  $(x, y, w, h, \alpha_1, \alpha_2, \alpha_3, \alpha_4)$  contributes a lot to the improvement. The proposed detection scheme brings 0.59% and 1.06% mAP improvement with and without FPN [3], respectively. When larger IoU threshold 0.7 is used, the selection scheme yields 2.55% mAP improvement.

#### 4.4 Long text detection in natural scenes

For oriented scene text detection on MSRA-TD500 [39] and RCTW-17 [40], we apply the same data augmentation as

TABLE 3

Quantitative comparison with other methods on MSRA-TD500 [39]. MS stands for multi-scale test.

Methods	Precision	Recall	F-measure	FPS
Zhang <i>et al.</i> [12]	83.0	67.0	74.0	0.5
SegLink [9]	86.0	70.0	77.0	8.9
RRD [34]	87.0	73.0	79.0	10.0
EAST [4]	87.3	67.4	76.1	13.2
Border MS [49]	83.0	73.3	76.8	-
TextField [31]	87.4	75.9	81.3	5.2
Lyu <i>et al.</i> [10]	87.6	76.2	81.5	5.7
MCN [11]	88.0	79.0	83.0	-
Wang <i>et al.</i> [48]	85.2	82.1	83.6	10.0
Direct MS [7]	<b>91.0</b>	81.0	86.0	-
Ours	88.8	<b>84.3</b>	<b>86.5</b>	<b>15.0</b>

TABLE 4

Quantitative comparison with other methods on RCTW-17 [40]. MS stands for multi-scale test.

Methods	Precision	Recall	F-measure	FPS
Official baseline [40]	76.0	40.4	52.8	8.9
RRD [34]	72.4	45.3	55.7	10.0
RRD MS	77.5	59.1	67.0	-
Direct MS [7]	76.7	57.9	66.0	-
Border MS [49]	78.2	58.8	67.1	-
LOMO [8]	<b>80.4</b>	50.8	62.3	4.4
LOMO MS	79.1	60.2	68.4	-
Ours	77.0	61.0	68.1	7.8
Ours MS	77.6	<b>62.7</b>	<b>69.3</b>	-

SSD [20]. Besides, we also randomly rotate the images with  $\pi/2$  to better handle vertical texts. The training images are randomly cropped and resized to some specific sizes. For MSRA-TD500, we randomly resize the short side of cropped images to  $\{512, 768, 864\}$ . For RCTW-17 [40] containing many small texts, the short side is randomly resized to  $\{960, 1200, 1400\}$ . We first pre-train the model on Synth-Text [47] for one epoch. Then we fine-tune the model for  $4k$  (*resp.*  $14k$ ) and decay the learning rate at  $3k$  (*resp.*  $10k$ ) steps for MSRA-TD500 (*resp.* RCTW-17). During test, the short side of MSRA-TD500 images is resized to 768. For RCTW-17, the short side is set to 1200 for single scale test. We add extra scales of  $\{512, 1024, 1280, 1560\}$  for multi-scale test.

Some qualitative illustrations are given in Fig. 5(b-e). The proposed method correctly detect texts of arbitrary orientations. The quantitative comparisons with some state-of-the-art methods on MSRA-TD500 and RCTW-17 are depicted in Tab. 3 and Tab. 4, respectively. The proposed method outperforms other competing methods and is more efficient on both datasets. Specifically, on MSRA-TD500, the proposed method under single scale test outperforms the multi-scale version of [7] using larger extra training images by 0.5%, and improves [48] by 2.9%. On RCTW-17, the proposed method outperforms the state-of-the-art method [8] by 5.8% (*resp.* 0.9%) under single-scale (*resp.* multi-scale) test while being much more efficient.

#### 4.5 Pedestrian detection in fisheye images

We compare the proposed method with baseline methods using quadrangle regression and classical horizontal box regression on MW-18Mar [41]. All images are resized to  $1024 \times 1024$ . We randomly rotate the images during training phase for data augmentation. The model is trained in total for  $4k$  steps and the learning rate decays at  $3k$  steps.

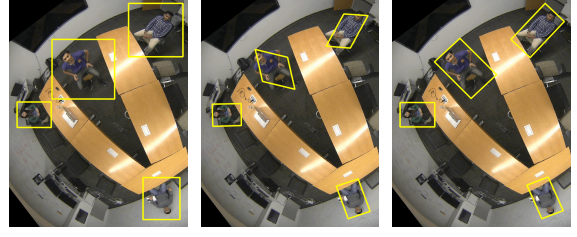


Fig. 7. Qualitative illustrations of different methods on MW-18Mar [41].

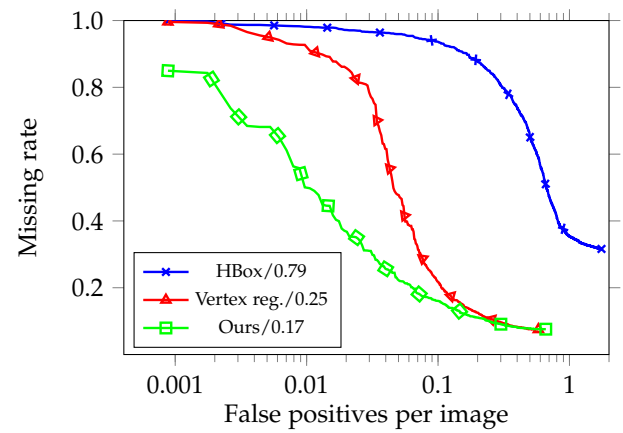


Fig. 8. Evaluation on MW-18Mar [41]. The numbers are the LAMRs.

Some qualitative results are illustrated in Fig. 7. Horizontal pedestrian detection denoted by HBox does not accurately enclose pedestrians. the proposed method achieves more accurate results than the baseline methods. The curve of missing rate with respect to number of false positives per image is depicted in Fig. 8. The proposed method achieves lower missing rate.

## 5 CONCLUSION

In this paper, we propose a simple yet effective representation for oriented objects and a divide-and-conquer strategy to detect multi-oriented objects. Based on this, we build a robust and fast multi-oriented object detector. It accurately detects ubiquitous multi-oriented objects such as objects in aerial images, scene texts, and pedestrians in fisheye images. Extensive experiments demonstrate that the proposed method outperforms some state-of-the-art methods on multiple benchmarks while being more efficient. In the future, we would like to explore the complementary of the proposed method with other approaches focusing on feature enhancement. One-stage multi-oriented object detector is also another direction which is worthy of exploitation.

## REFERENCES

- [1] S. Ren, K. He, R. Girshick, and J. Sun, "Faster R-CNN: Towards real-time object detection with region proposal networks," *IEEE Trans. on Pattern Anal. and Mach. Intell.*, no. 6, pp. 1137–1149, 2017.
- [2] J. Redmon and A. Farhadi, "YOLOv3: An incremental improvement," *arXiv preprint arXiv:1804.02767*, 2018.
- [3] T.-Y. Lin, P. Dollár, R. Girshick, K. He, B. Hariharan, and S. Belongie, "Feature pyramid networks for object detection," in *Proc. of IEEE Intl. Conf. on Computer Vision and Pattern Recognition*, 2017, pp. 2117–2125.

- [4] X. Zhou, C. Yao, H. Wen, Y. Wang, S. Zhou, W. He, and J. Liang, "EAST: An efficient and accurate scene text detector," in *Proc. of IEEE Intl. Conf. on Computer Vision and Pattern Recognition*, 2017, pp. 2642–2651.
- [5] J. Ding, N. Xue, Y. Long, G.-S. Xia, and Q. Lu, "Learning roi transformer for oriented object detection in aerial images," in *Proc. of IEEE Intl. Conf. on Computer Vision and Pattern Recognition*, 2019, pp. 2849–2858.
- [6] M. Liao, B. Shi, and X. Bai, "Textboxes++: A single-shot oriented scene text detector," *IEEE Trans. on Image Processing*, vol. 27, no. 8, pp. 3676–3690, 2018.
- [7] W. He, X.-Y. Zhang, F. Yin, and C.-L. Liu, "Multi-oriented and multi-lingual scene text detection with direct regression," *IEEE Trans. on Image Processing*, vol. 27, no. 11, pp. 5406–5419, 2018.
- [8] C. Zhang, B. Liang, Z. Huang, M. En, J. Han, E. Ding, and X. Ding, "Look more than once: An accurate detector for text of arbitrary shapes," *Proc. of IEEE Intl. Conf. on Computer Vision and Pattern Recognition*, pp. 10552–10561, 2019.
- [9] B. Shi, X. Bai, and S. Belongie, "Detecting oriented text in natural images by linking segments," in *Proc. of IEEE Intl. Conf. on Computer Vision and Pattern Recognition*, 2017, pp. 3482–3490.
- [10] P. Lyu, C. Yao, W. Wu, S. Yan, and X. Bai, "Multi-oriented scene text detection via corner localization and region segmentation," in *Proc. of IEEE Intl. Conf. on Computer Vision and Pattern Recognition*, 2018, pp. 7553–7563.
- [11] Z. Liu, G. Lin, S. Yang, J. Feng, W. Lin, and W. L. Goh, "Learning markov clustering networks for scene text detection," in *Proc. of IEEE Intl. Conf. on Computer Vision and Pattern Recognition*, 2018, pp. 6936–6944.
- [12] Z. Zhang, C. Zhang, W. Shen, C. Yao, W. Liu, and X. Bai, "Multi-oriented text detection with fully convolutional networks," in *Proc. of IEEE Intl. Conf. on Computer Vision and Pattern Recognition*, 2016, pp. 4159–4167.
- [13] Z.-Q. Zhao, P. Zheng, S.-t. Xu, and X. Wu, "Object detection with deep learning: A review," *IEEE Trans. on Neural Networks and Learning Systems*, 2019.
- [14] R. Girshick, J. Donahue, T. Darrell, and J. Malik, "Rich feature hierarchies for accurate object detection and semantic segmentation," in *Proc. of IEEE Intl. Conf. on Computer Vision and Pattern Recognition*, 2014, pp. 580–587.
- [15] R. Girshick, "Fast R-CNN," in *Proc. of IEEE Intl. Conf. on Computer Vision*, 2015, pp. 1440–1448.
- [16] J. R. Uijlings, K. E. Van De Sande, T. Gevers, and A. W. Smeulders, "Selective search for object recognition," *International Journal of Computer Vision*, vol. 104, no. 2, pp. 154–171, 2013.
- [17] J. Dai, Y. Li, K. He, and J. Sun, "R-FCN: Object detection via region-based fully convolutional networks," in *Proc. of Advances in Neural Information Processing Systems*, 2016, pp. 379–387.
- [18] J. Redmon, S. Divvala, R. Girshick, and A. Farhadi, "You only look once: Unified, real-time object detection," in *Proc. of IEEE Intl. Conf. on Computer Vision and Pattern Recognition*, 2016, pp. 779–788.
- [19] J. Redmon and A. Farhadi, "YOLO9000: Better, faster, stronger," in *Proc. of IEEE Intl. Conf. on Computer Vision and Pattern Recognition*, 2017, pp. 7263–7271.
- [20] W. Liu, D. Anguelov, D. Erhan, C. Szegedy, S. Reed, C.-Y. Fu, and A. C. Berg, "SSD: Single shot multibox detector," in *Proc. of European Conference on Computer Vision*, 2016, pp. 21–37.
- [21] T.-Y. Lin, P. Goyal, R. Girshick, K. He, and P. Dollár, "Focal loss for dense object detection," in *Proc. of IEEE Intl. Conf. on Computer Vision*, 2017, pp. 2980–2988.
- [22] H. Law and J. Deng, "CornerNet: Detecting objects as paired keypoints," in *Proc. of European Conference on Computer Vision*, 2018, pp. 734–750.
- [23] X. Zhou, J. Zhuo, and P. Krahenbuhl, "Bottom-up object detection by grouping extreme and center points," in *Proc. of IEEE Intl. Conf. on Computer Vision and Pattern Recognition*, 2019, pp. 850–859.
- [24] K. Duan, S. Bai, L. Xie, H. Qi, Q. Huang, and Q. Tian, "CenterNet: Object detection with keypoint triplets," *arXiv preprint arXiv:1904.08189*, 2019.
- [25] G.-S. Xia, X. Bai, J. Ding, Z. Zhu, S. Belongie, J. Luo, M. Datcu, M. Pelillo, and L. Zhang, "DOTA: A large-scale dataset for object detection in aerial images," in *Proc. of IEEE Intl. Conf. on Computer Vision and Pattern Recognition*, 2018, pp. 3974–3983.
- [26] L. Liu, Z. Pan, and B. Lei, "Learning a rotation invariant detector with rotatable bounding box," *arXiv preprint arXiv:1711.09405*, 2017.
- [27] Z. Zhang, W. Guo, S. Zhu, and W. Yu, "Toward arbitrary-oriented ship detection with rotated region proposal and discrimination networks," *IEEE Geoscience and Remote Sensing Letters*, no. 99, pp. 1–5, 2018.
- [28] S. M. Azimi, E. Vig, R. Bahmanyar, M. Körner, and P. Reinartz, "Towards multi-class object detection in unconstrained remote sensing imagery," in *Asian Conference on Computer Vision*, 2018, pp. 150–165.
- [29] X. Yang, K. Fu, H. Sun, J. Yang, Z. Guo, M. Yan, T. Zhan, and S. Xian, "R2CNN++: Multi-dimensional attention based rotation invariant detector with robust anchor strategy," *arXiv preprint arXiv:1811.07126*, 2018.
- [30] G. Zhang, S. Lu, and W. Zhang, "CAD-Net: A context-aware detection network for objects in remote sensing imagery," *arXiv preprint arXiv:1903.00857*, 2019.
- [31] Y. Xu, Y. Wang, W. Zhou, Y. Wang, Z. Yang, and X. Bai, "Textfield: Learning a deep direction field for irregular scene text detection," *IEEE Trans. on Image Processing*, 2019.
- [32] J. Ma, W. Shao, H. Ye, L. Wang, H. Wang, Y. Zheng, and X. Xue, "Arbitrary-oriented scene text detection via rotation proposals," *IEEE Trans. on Multimedia*, 2018.
- [33] Y. Liu and L. Jin, "Deep matching prior network: Toward tighter multi-oriented text detection," in *Proc. of IEEE Intl. Conf. on Computer Vision and Pattern Recognition*, 2017, pp. 3454–3461.
- [34] M. Liao, Z. Zhu, B. Shi, G. Xia, and X. Bai, "Rotation-sensitive regression for oriented scene text detection," in *Proc. of IEEE Intl. Conf. on Computer Vision and Pattern Recognition*, 2018, pp. 5909–5918.
- [35] R. Seidel, A. Apitzsch, and G. Hirtz, "Omnidetector: With neural networks to bounding boxes," *arXiv preprint arXiv:1805.08503*, 2018.
- [36] M. Tamura, S. Horiguchi, and T. Murakami, "Omnidirectional pedestrian detection by rotation invariant training," in *Proc. of IEEE Winter Conf. on Applications of Computer Vision*, 2019, pp. 1989–1998.
- [37] K. He, G. Gkioxari, P. Dollár, and R. Girshick, "Mask R-CNN," in *Proc. of IEEE Intl. Conf. on Computer Vision*, 2017, pp. 2980–2988.
- [38] Z. Liu, H. Wang, L. Weng, and Y. Yang, "Ship rotated bounding box space for ship extraction from high-resolution optical satellite images with complex backgrounds," *IEEE Geoscience and Remote Sensing Letters*, vol. 13, no. 8, pp. 1074–1078, 2016.
- [39] C. Yao, X. Bai, W. Liu, Y. Ma, and Z. Tu, "Detecting texts of arbitrary orientations in natural images," in *Proc. of IEEE Intl. Conf. on Computer Vision and Pattern Recognition*, 2012, pp. 1083–1090.
- [40] B. Shi, C. Yao, M. Liao, M. Yang, P. Xu, L. Cui, S. Belongie, S. Lu, and X. Bai, "ICDAR2017 competition on reading chinese text in the wild (RCTW-17)," in *Proc. of International Conference on Document Analysis and Recognition*, vol. 1, 2017, pp. 1429–1434.
- [41] Mirror worlds challenge. [Online]. Available: <https://icat.vt.edu/mirrorworlds/challenge/index.html>
- [42] C. Yao, X. Bai, and W. Liu, "A unified framework for multioriented text detection and recognition," *IEEE Trans. on Image Processing*, vol. 23, no. 11, pp. 4737–4749, 2014.
- [43] P. Dollar, C. Wojek, B. Schiele, and P. Perona, "Pedestrian detection: An evaluation of the state of the art," *IEEE Trans. on Pattern Anal. and Mach. Intell.*, vol. 34, no. 4, pp. 743–761, 2011.
- [44] K. He, X. Zhang, S. Ren, and J. Sun, "Deep residual learning for image recognition," in *Proc. of IEEE Intl. Conf. on Computer Vision and Pattern Recognition*, 2016, pp. 770–778.
- [45] Z. Li, C. Peng, G. Yu, X. Zhang, Y. Deng, and J. Sun, "Light-Head R-CNN: In defense of two-stage object detector," *arXiv preprint arXiv:1711.07264*, 2017.
- [46] Z. Liu, J. Hu, L. Weng, and Y. Yang, "Rotated region based cnn for ship detection," in *Proc. of IEEE Intl. Conf. on Image Processing*, 2017, pp. 900–904.
- [47] A. Gupta, A. Vedaldi, and A. Zisserman, "Synthetic data for text localisation in natural images," in *Proc. of IEEE Intl. Conf. on Computer Vision and Pattern Recognition*, 2016, pp. 2315–2324.
- [48] X. Wang, Y. Jiang, Z. Luo, C.-L. Liu, H. Choi, and S. Kim, "Arbitrary shape scene text detection with adaptive text region representation," in *Proc. of IEEE Intl. Conf. on Computer Vision and Pattern Recognition*, 2019, pp. 6449–6458.
- [49] C. Xue, S. Lu, and F. Zhan, "Accurate scene text detection through border semantics awareness and bootstrapping," in *Proc. of European Conference on Computer Vision*, 2018, pp. 355–372.